J Mater Sci: Mater Med (2007) 18:1497–1506
DOI 10.1007/s10856-007-0128-z

Influence of acid washing on the surface morphology of ionomer glasses and handling properties of glass ionomer cements

C. M. Crowley · J. Doyle · M. R. Towler · N. Rushe · S. Hampshire

Received: 13 October 2005 / Accepted: 8 March 2006 / Published online: 27 March 2007
© Springer Science+Business Media, LLC 2007

Abstract Acid washing is known to influence the handling properties of ionomer glasses used in glass ionomer cements due to the production of an ion depleted-zone on the surface of the glass particles. The influence of acid washing on the particle size distribution and surface area of four glasses was examined by scanning electron microscopy (SEM), particle size analysis (PSA) and accelerated surface area porosimetry (ASAP) and the working and setting times of cements, produced from the glasses, correlated to changes in surface morphology. A linear relationship was found between the specific surface area of acid-washed SiO_2–Al_2O_3–XF_2–P_2O_5 glasses (X being either calcium or strontium) and their cement working and setting times. These changes directly correlated with increases in the mesopore volume. However, the influence of acid washing on the surface morphology was also found to be glass composition-dependant with the addition of sodium into the glass network resulting in no significant change in the surface area or mesopore volume despite changes in the working and setting time. Through examination of the influence of acid washing and glass composition on the specific surface area improvements in the control of the working and setting times of glass ionomer cements may be achieved.

C. M. Crowley (✉) · J. Doyle · S. Hampshire
Materials Ireland Research Centre, University of Limerick, National Technological Park, Limerick, Ireland
e-mail: Clare.Crowley@ul.ie

M. R. Towler · N. Rushe · S. Hampshire
Materials and Surface Science Institute, University of Limerick, National Technological Park, Limerick, Ireland

1 Introduction

Glass ionomer cements (GICs), or glass polyalkenoate cements (GPCs), are acid-based cements that are formed by reacting a poly(carboxylate) (e.g. poly (acrylic acid) (PAA) or acrylic/maleic acid copolymer) in an aqueous environment with an ion-leachable acid-degradable glass of the generic form SiO_2–Al_2O_3–XF_2 glass (X being any bivalent cation) [1] to produce a crosslinked hydrogel matrix in which the glass-filler phase is embedded. The main advantages of these cements are that setting is not associated with a significant exothermic reaction or shrinkage and, due to their hydrophilicity, they are able to directly bond to the apatite crystals in the dental tissue producing an excellent chemical seal along the cement–substrate interface [2, 3]. Additional benefits of GICs are their aesthetics [4] and their propensity to liberate fluoride ions, which has been shown to be cariostatic [5].

A major disadvantage of the glass ionomer cements resides is their sensitivity to water during and after setting. This water sensitivity is unavoidable during the early stages of setting (working time (WT)) but by increasing the rate of set the time-period associated with the post-setting water sensitivity (setting time (ST)) can be significantly reduced. These time scales must allow a sufficiently long working time to enable placement and shaping of the cement paste in the mouth whilst the setting times would ideally be instantaneous following placement. The cement-forming ability of a glass and the rate of setting of conventional GPCs are primarily dependent on the susceptibility of the glass to acid-degradation during the setting reaction which controls the handling properties of the cement paste (working and setting times)

and ultimately determines the mechanical properties of the cements [6].

The ionomer glasses are synthesised by fusing the powdered constituents of the glass at a high temperature (typically in excess of 1,400 °C) to produce a molten mass that is then shock-cooled and subsequently finely ground to a powder before use. Although the composition of the glasses varies they are generally based on three main components: silica and alumina that are mixed in a flux of calcium, strontium or lanthanum fluoride. Many of the commercial glasses also contain sodium and aluminium fluorides and calcium or aluminium phosphates as additional fluxes to aid glass synthesis. Due to the clinical requirement for radio-opaque materials, calcium is frequently replaced by radio-opacifiers such as strontium and lanthanum.

Glass behaviour has been predicted in terms of their surface reactivity, solubility and glass transition temperature (Tg) on the basis of their network connectivity (NC) [7], or crosslink density (CLD) (i.e. the lower the CLD the lower the degree of polymerisation of the glass structure, Tg and melting temperature (Tm) and the greater their reactivity and solubility), whilst the rate of set of the cements has been correlated to the acid–base characteristics of the glass (net charge balance (NCB)) with the rate of set reportedly increasing with increasing glass basicity [8].

The Si atoms in the glass network are assumed to be in tetrahedral co-ordination state, neutralised by four oxygen atoms. Si is partially replaced by aluminium in a four-fold co-ordination state if the Al:Si ratio is <1:1. However, the Al:Si ratio of the ionomer glasses tends to be between 1.5 and 2, compared to 1:1 in silicate cements, which results in a reduction in the WT and the inclusion of Al^{V} and Al^{VI} species in the glass network [9]. Phosphorus in the glass network acts in a manner analogous to silicon, charge balancing aluminium, whilst mono- and/or divalent cations (e.g. Na^{+}, Ca^{2+}, Sr^{2+}) behave in two ways within the glass network: either as network dwelling cations charge balancing the aluminium ions or as network modifiers effectively depolymerising the silica network structure due to the creation of non-bridging oxygens (NBOs) [10]. An increase in the number of NBOs increases the degradability of the glass and reduces the CLD effectively reducing the Tg and Tm of the glass network. The alkali metal ions are the most effective in disrupting the glass network thus aiding glass synthesis (due to the reduction in the CLD and consequently the Tg and Tm) but their presence also increases the basicity of the glass, increasing the susceptibility of the glass to acid degradation thereby reducing the WT and ST of the ionomer cement paste. A further drawback of the use of alkali metal ions is that their presence also unfavourably influences the water-resistivity of the cements during the early stages of setting, which can lead to surface clouding and deterioration in the translucency, thus effectively reducing the aesthetic characteristics of the cement. The inclusion of additional network modifiers, such as fluorine, aids glass synthesis and also influences the working and setting times of the cements as a function of the fluorine content due to the concomitant disruption of the glass network and increase in the basicity of the glass [11].

Approaches to improving rheology and, therefore, better mixing manipulation of GPC pastes, have been achieved by heat- and surface-treatments of the glass powder. Heat treatment decreases the glass reactivity [12], improves the handling characteristics of the mixed cement and, under some conditions, increases the compressive strength [13]. Modification of the surface of the glass particles has been achieved by silanisation and acid washing, which extend the working time of the cements without significantly influencing the setting time by inducing a delay in the ion leaching process [14].

In the latter approach the glass particles are washed in a mildly acidic solution, e.g. acetic acid, to produce a surface layer depleted of cations. The depth of this depletion-zone depends on the acid washing procedure and the glass composition but, in practice, the glasses are treated such that the working time of the cement paste is at least 1.5 min at 23 °C. This reportedly corresponds to a depletion-zone depth of approximately 100 nm for dental filling applications [15]. Quantitative differences in acid degradability of ionomer glasses have been correlated with their mean chemical composition and with the rate of the setting reaction, which increases with an increasing ratio of network-dwelling cations to Al^{3+} ions [16]. It has been proposed that acid hydrolysis of the Al–O–Si bonds and the extraction of metal cations results in an increase in the number of non-bridging oxygens (NBOs) in the glass network at the glass particle surface with the production of a surface rich in silanols (–Si–OH). However, studies using SIMS/MAS-NMR [17] and ESCA [15], which examined the influence of acid washing on calcium phospho-alumino-silicate glasses, show that Al and Ca ions are lost from the glass surface leaving a silicon- and phosphorus-rich surface layer irrespective of the strength of the acid washing media. The inclusion of sodium in the glass on the other hand leads to the enhanced release of Na^{+} ions in dilute acid but when the acidity of the media is

increased (e.g. 0.1 M HCl), stoichiometric leaching equivalent to that of the bulk glass composition occurs [14, 18–20].

Examination of the influence of the glass phosphorus content on the handling properties of GICs has shown that increasing phosphorus content increases the working time of the cement paste but does not necessarily result in an increase in the cement strength [21], while exposure of ionomer glass to a phosphate solution dramatically increases the cement working time [22]. Although these studies indicate the pivotal role of phosphorus/phosphate in controlling the working time of GICs the mechanism of this behaviour is unclear.

It is apparent that the handling properties (WT and ST) of glass ionomer cements are dependant on the relative proportions of the constituents of the glass, due to their various influences on the acid degradability and leaching characteristics at the glass–solution interface and therefore that the handling characteristics of GICs can be significantly modified by manipulating the glass composition [23, 24] or by surface modification of the glass [14, 15, 18, 20, 25] e.g. acid washing of ionomer glasses reduces the rate of the initial ion-release which delays the onset of crosslinking and hence extends the working time. Alternatively the setting reaction, and hence the handling properties, can be modified by controlling the particle size distribution [26–28], powder:liquid ratio [29] and by including (+)-tartaric acid [30, 31]. For dental filling materials the optimum average particle size (weight average) is preferably 3–10 μm with a maximum particle size of 50 μm [1, 15], a BET specific surface area of 2.5–6.0 m^2/g [32], powder:liquid ratio in excess of 7:1 and approximately 10%-w/w (+)-tartaric acid of the powder fraction.

In the cement systems, the setting of GICs is brought about by acidic degradation of the glass network on the surface of the glass particles in conjunction with the ionisation of the carboxylic acid moieties of the poly(carboxylic acid). This results in the formation of H_3O^+, which attacks the fluoro-alumino-silicate glass releasing metal cations and fluoride anions (e.g. Ca^{2+}, Al^{3+}, Na^+ and F^-) producing a silica-rich hydrogel layer on the surface of the glass particles. The liberated divalent and trivalent cations (e.g. Ca^{2+} and Al^{3+}) act as crosslinks or bridges between the carboxylate anions on the polyacid chains resulting in the production of an ionically crosslinked hydrogel poly(salt) matrix [33, 34]. Acid washing of the glasses reduces the rate of this initial ion-release, delaying the onset of crosslinking and hence extending the working time. A secondary hardening mechanism that contributes to the increase in the cement properties with maturation time also occurs. This has been attributed to the formation of hydrated silicates in the matrix [35, 36] a view not universally accepted [37, 38].

As the glass component critically determines the properties of GPCs, the relationship between the composition of the glass and these properties is examined. To investigate this relationship the change in the particle size distribution, surface area, surface porosimetry and the reactivity of glasses used in experimental GPCs, pre- and post-acid washing in acetic acid solutions, has been examined. Quantitative differences in the surface porosimetry and correlation of these values with the working and setting times of cements have been compared and are discussed.

2 Methods

2.1 Glass synthesis

Glasses A, B and C were synthesised according to the compositions described in Table 1. A commercial glass, glass D, pre-firing composition unknown, (supplied by Advanced Healthcare Limited (AHL) (Tonbridge, UK)) was used as received. The post-melt compositions and thermal properties of the three synthesised experimental glasses and the commercial glass were determined by XRF and DTA, respectively.

Appropriate amounts of analytical grade reagents were mixed by rotation for 1 h and then dried in a vacuum oven (100°C, 1 h) prior to being transferred into a dense sintered mullite crucible (Zedmark, UK). The glasses were then fired in a muffle furnace (Elite BRF16/21) at between 1,420 °C and 1,470 °C for

Table 1 Pre-firing constituent molar ratios and wt% compositions of the experimental glasses

Glass	Molar ratios							Wt (%)						
	SiO_2	Al_2O_3	P_2O_5	CaF_2	SrO	SrF_2	Na_2O	SiO_2	Al_2O_3	P_2O_5	CaF_2	SrO	SrF_2	Na_2O
A	4.5	3	1.5	2	3	–	–	21.50	24.37	16.96	12.42	24.75	–	–
B	4.5	3	1.5	–	3	2	–	20.00	22.67	15.78	–	23.03	18.52	–
C	4.5	3	0.75	–	3	2	–	21.72	24.61	8.57	–	25.00	20.11	–

one-and-a-half to two hours. The glass melts were then shock quenched into demineralised water. The resulting frit was dried, ground by milling and wet sieved. (Glasses produced by milling are designated subscript M.)

The crosslink density (CLD) and the net charge balance (NCB) of the post-melt glass compositions were calculated using Eqs. (1) and (2).

$$\mathrm{CLD} = \frac{(2 \times \text{Total number of bridging oxygen}) - \text{number broken by modifiers}}{\text{Total number of possible bridges}} \quad (1)$$

$$\mathrm{NCB} = \sum\left(\text{Ionic Charge}\left(\frac{\text{Elemental weight contribution}}{\text{Relative Molecular Mass}}\right)\right) \quad (2)$$

2.2 Acid treatment procedure

Following milling the glass powders were acid-washed by mixing de-ionised water (67 mL) with the glass (20 g) followed by the addition of 10 mL of acetic acid (either 2.5 vol% or 5 vol% glacial acetic acid). (Glasses produced by these two acid washing treatments are designated with subscripts AW1 and AW2, respectively.) The dispersion was stirred for 1 h and then left to stand for 24 h after which the dispersion was filtered under vacuum and the glass particles washed thoroughly with de-ionised water, oven dried (120 °C, 2 h) and sieved (<45 μm) prior to use.

2.3 X-ray fluorescence (XRF)

The XRF data was supplied by Advanced Healthcare Limited (AHL) (Tonbridge, UK) and results are presented in Table 4.

2.4 Differential thermal analysis (DTA)

The mid-point glass transition temperature (Tg), peak crystallisation temperatures (Tp_1 and Tp_2) and melting temperatures (Tm) of the glasses were analysed using a Stanton Redcroft STA 780 (Rheometric Scientific, Epsom, Surrey). A total of 50 mg of glass was heated at 10 °C/min from 100 °C to 1,500 °C under air.

2.5 Particle size analysis

A stable glass dispersion, suspended in 0.1%-w/v Calgon (Sodium Hexametaphosphate), was added to the Hydro2000 (A) chamber of a Mastersizer 2000 (Malvern Instruments, Worcs., UK) until an obscuration value of between 10% and 15% was obtained. The milled and acid-washed samples were examined under the same conditions (stirrer speed of 2,600 rpm, 0% or 10% ultrasonics), using solvent and glass refractive indices (RI) of 1.33 and 1.52, respectively, and a particle absorption index (PAI) of 0.0001. The RI and PAI of the glasses were used to calculate the particle size analysis fit model that is based on the Mie theory, the closeness of the fit of the model to the test sample distribution being indicative of the accuracy of the analysis data [39].

2.6 Surface area and porosimetry analysis

Surface area and porosimetry analyses were performed on a Micromeritics® ASAP 2010 system under the specified conditions and conversion factors given in Table 2. The system performs automatic single-point and multi-point BET surface area, full adsorption and desorption isotherms and pore size and pore volume distributions. The sample weight was altered to ensure 8–12 m^2 was presented for nitrogen adsorption [40, 41]. Samples were placed in standard sample tubes and were outgassed at 60 °C for at least 12 h to obtain a residual pressure less than 10^{-3} torr prior to analysis.

Nitrogen adsorption and desorption isotherms were measured at 77 K, and the surface areas determined using the BET equation (Eq. (3)a and b). The pore size distribution curves were obtained from the analysis of the desorption branch of the nitrogen isotherm using the BJH method and the pore volumes were reduced to their corresponding liquid nitrogen volumes using a density conversion factor of 1.5468×10^{-3} [40–42].

Table 2 Surface area analysis conditions

Adsorptive	Nitrogen at 77.35 K
Maximum manifold pressure	925 mmHg
Non-ideality factor	0.000066
Density conversion factor	0.0015468
Therm. tran. hard-sphere diameter	3.860 Å
Molecular cross-sectional area	0.162 nm^2
BET Linear range	0.05–0.2

$$n/n_m = c(P/P_o)/[(1 - P/P_o)(1 + (c - 1)(P/P_o)] \quad (3a)$$

or

$$P/[n(P_o - P)] = 1/n_m c + [(c - 1)/n_m c][P/P_o] \quad (3b)$$

where, n = the moles of gas adsorbed at the equilibrium pressure P/P_o; n_m = the moles of gas adsorbed at the monolayer capacity; P_o = vapour pressure of the adsorbate; P = gas pressure; c = a constant, which is related exponentially to the "first layer" heat of adsorption or more correctly may be regarded as a free energy term:

$$c = \exp[(q_l - q_L)/RT] \quad (4)$$

where, $(q_l - q_L)$ = the net heat of adsorption; R = the ideal gas law constant (1.9872 cal K^{-1} mol^{-1}); T = the absolute temperature (K).

2.7 Cement preparation

Cements were formulated by mixing reagents in the following ratios: glass (82.6 wt%), PAA_{50} (16.0 wt%) and (+)-tartaric acid (1.4 wt%) with de-ionised water at a powder:liquid (P:L) ratio of 7:1 on a glass plate. Complete mixing was undertaken within 30 s. The molecular weight distribution of the anhydrous PAA_{50} is presented in Table 3 and was supplied by Advanced Healthcare Limited (AHL) (Tonbridge, UK). The so-formed cements are named after the glass phase from which they formed (i.e. cement A is formulated from glass A) with the subscripts M, AW1 and AW2 indicating whether the glasses have been milled only (M) or acid-washed.

Table 3 Weight- and number- average molecular weight ($\overline{M}_w$ and $\overline{M}_n$, respectively) and polydispersity (P.D.) of the poly (acrylic acid) (PAA)

PAA	GPC data		
	$\overline{M}_w$	$\overline{M}_n$	P.D.
PAA_{50}	51,900	21,900	2.4

2.8 Determination of working and setting times

The working and setting times of the cements were measured in accordance with ISO9917E [43]. The mean setting time of three tests was recorded.

3 Results

For the experimental glasses A and B the pre-melt molar compositions were varied only in the degree of calcium substitution by strontium; whilst for glass C the phosphate content was halved as compared with glass B. Therefore, it was expected that, based on their pre-fired compositions, that glasses A and B would possess the same R^{2+}:P and CLD values whilst the R^{2+}:P ratio of glass C would be double that of glass B with a consequential increase in the CLD. Tables 4 and 5 compares the pre- and post-melt glass compositions, as evaluated by XRF, showing an increase in the Al:Si ratio due to the loss of silicon tetrafluoride during firing, whilst the thermal properties of the glasses are presented in Table 6.

The calculated CLD of glass A was significantly less than those of glasses B and C resulting in a reduction in the Tg as predicted by the Gibbs–De Marzio equation [44], while the incorporation of sodium into glass D caused an expected reduction in the Tg compared to glasses B and C which possess similar CLDs. While weight loss from the glasses A, B and C, attributed to SiF_4 loss, increased as Tg increased with A < B < C.

Dispersion of the glasses in water resulted in aggregation of glass C particles that was negated by dispersion in Calgon and PBS (data not shown). Flocculation of bioactive glasses has been attributed

Table 4 Calculated equivalent percent composition of the pre-melt glasses compared with the post-melt glasses as determined by XRF analysis

Glass		Equivalent Wt-% Composition						
		SiO_2	Al_2O_3	P_2O_5	CaO	SrO	Na_2O	F
Pre-firing	A	21.50	24.37	16.96	6.38	24.75	–	6.04
	B	20.00	22.67	15.78	–	35.95	–	5.60
	C	21.72	24.61	8.57	–	39.03	–	6.08
Post-firing	A	21.0	24.6	17.7	6.43	24.8	–	5.0
	B	19.5	23.1	16.7	–	38.4	–	4.5
	C	21.4	25.7	9.3	–	39.8	–	5.3
	D	29.5	26.8	5.9	–	24.9	2.2	10.6

Table 5 Comparison of the influence of firing of the glasses on the calculated pre- and post-melt molar ratio compositions and its influence on the glass network structure

Glass		Molar ratios								R^{2+}:P	Al:Si	NCB	CLD
		SiO_2	Al_2O_3	P_2O_5	CaO	CaF_2	SrO	SrF_2	NaF				
Pre-firing	A	4.5	3	1.5	–	2	3	–	–	1.67	1.33	0.63	1.19
	B	4.5	3	1.5	–	–	3	2	–	1.67	1.33	0.45	1.19
	C	4.5	3	0.75	–	–	3	2	–	3.33	1.33	0.85	1.21
Post-firing	A	4.5	3.1	1.6	0.4	1.7	3.1	–	–	1.63	1.38	0.69	1.11
	B	4.5	3.1	1.6	–	–	3.5	1.7	–	1.63	1.38	0.46	1.30
	C	4.5	3.2	0.8	–	–	3.2	1.8	–	3.13	1.42	0.94	1.28
	D	4.5	2.4	0.4	–	–	–	2.2	0.6	2.75	1.07	0.43	1.30

Table 6 Comparison of the thermal behaviour of the post-melt glasses. Glass particle size <45 μ

Glass	%-Wt Loss*	Tg (°C)	Tp_1 (°C)	Tp_2 (°C)	Tm (°C)
A	0.6	624	769	815	1420
B	1.3	649	814	nd	1420
C	2.5	651	742	nd	1490
D	4.6	552	686	705	–

nd = not detected; *Weight loss under air between 100 °C and 800 °C

to the formation of a charged surface on the glass particles (from zeta potential measurements) due to the uptake of calcium and phosphate at the glass–solution interface [45, 46]. However, the phosphorus content of glass C is low. Therefore, aggregation/flocculation in water is likely to be a consequence of moisture uptake from the atmosphere resulting in hydrogen bond bridges being formed between the particles. The increased surface gloss of the glass C particles observed by SEM supports this (data not shown).

The PSD curves for all of the experimental glasses dispersed in 0.1% w/v Calgon showed monomodal distributions. An example of this is given in Fig. 1 for the milled experimental glass D. Comparison of the changes in the particle size distributions pre- and post-acid washing are presented in Table 7 and Fig. 2. The Mie specific surface area is the calculated surface area based on the PSD, which does not take into account surface roughness or porosity. For all of the glasses the calculated specific surface area increased and the d_{10} decreased as a consequence of acid washing. These changes correlate with an increase in the CLD of the glass and may be a consequence of particle fracturing during milling.

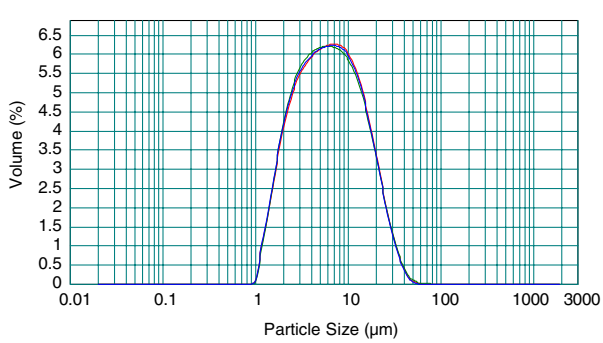

Fig. 1 Particle size distribution of the milled glass D (three overlayed averaged results each average taken from 10 consecutive runs)

The multi-point BET specific surface area of the glasses varied between 1.76 m^2/g and 4.36 m^2/g as indicated in Table 8 which, as illustrated in Fig. 2, was 200–400% greater than that predicted by the Mie specific surface area calculated from the change in the PSD. Acid washing resulted in an increase in the BET specific surface area of glasses A, B and C; whilst for glass D the milled glass had a greater surface area than the acid-washed glasses, which was reduced further when the strength of the acid-wash medium was increased.

Full adsorption–desorption isothermal analysis of the changes in the surface morphology of the milled and acid-washed glasses showed the glasses to have a low surface reactivity and a combination of Type II and Type IV behaviour (as classified by Brunauer, Doming, Deming and Teller (BDDT)), where Type II results from the physical adsorption of gases by non-porous solids and Type IV is from the physical adsorption of gases by mesoporous solids. A small closed hysteresis (Type H-2) was seen in the mesoporous range (i.e. 2–50 nm range) which was most pronounced with acid-washed glass C. It appears that the change in the specific surface area relates to these changes in the mesopore volume. Figures 3, 4 and 5 illustrate the changes in the pore volume fraction of the acid-washed glasses compared to the milled glasses.

For acid-washed glass C, five distinct pore distribution ranges appear as a consequence of acid washing:

Table 7 Comparison of the influence of acid washing on the particle size distribution (d_{10}, d_{50} and d_{90} are the 10, 50 and 90% particle diameter sizes calculated from the volume–% distribution curves)

Glass	Residual-weighted	d_{10} (μm)	d_{50} (μm)	d_{90} (μm)	Mie specific surface area (m^2/g)	Span ($d_{90} - d_{10}$)
	Mean (SD)	Mean (SD)	Mean (SD)	Mean (SD)	Mean (SD)	
A_M	0.34 (0.07)	2.17 (0.03)	5.79 (0.11)	15.76 (0.58)	0.59 (0.003)	13.59
A_{AW1}	0.27 (0.03)	1.85 (0.07)	6.11 (0.13)	16.85 (0.35)	0.64 (0.015)	15.00
B_M	0.23 (0.02)	1.76 (0.07)	5.08 (0.07)	14.01 (0.31)	0.75 (0.082)	12.25
B_{AW1}	0.52 (0.34)	1.60 (0.04)	4.91 (0.12)	13.78 (0.68)	0.99 (0.097)	12.18
C_M	0.26 (0.02)	1.08 (0.03)	4.59 (0.05)	13.35 (0.17)	1.04 (0.015)	12.27
C_{AW1}	0.24 (0.01)	1.06 (0.06)	4.43 (0.06)	13.08 (0.06)	1.07 (0.055)	12.02
D_M	0.52 (0.06)	2.07 (0.01)	6.14 (0.07)	18.53 (0.03)	0.58 (0.003)	16.46
D_{AW1}	0.58 (0.21)	2.03 (0.03)	5.97 (0.04)	17.20 (0.74)	0.59 (0.003)	15.17
D_{AW2}	0.40 (0.08)	1.96 (0.03)	6.17 (0.09)	18.83 (0.02)	0.60 (0.008)	16.87

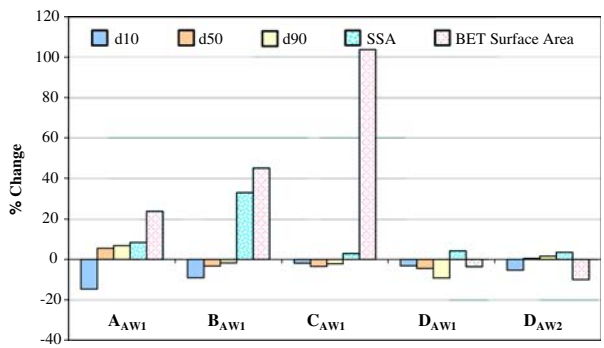

Fig. 2 Percentage change in the particle size distribution, the calculated Mie and measured BET specific surface area of the acid-washed glasses ($_{AW1}$ and $_{AW2}$: denotes glasses that have been acid washed in 2.5 vol% or 5 vol% glacial acetic acid, respectively)

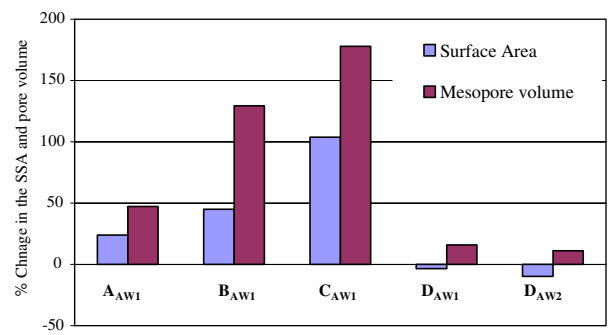

Fig. 3 The percentage change in the BET specific surface area and mesopore volume as a consequence of acid washing as compared with the milled glasses ($_{AW1}$ and $_{AW2}$: denotes glasses that have been acid washed in 2.5 vol% or 5 vol% glacial acetic acid, respectively)

a small number of micropores, several mesopore ranges (2.8–4.7, 4.7–11, 11–14.6 nm) and a broad meso-/macro-porous range (33–89 nm). Similar changes in the incremental pore volume distribution are seen with glasses A and B. For these three glasses acid washing appears to increase the pore volume for pores of less than 23 nm. This infers that acid washing of these glasses results in the selective degradation of small loci on the glass surface.

In comparison the adsorption isotherms for milled and acid washed glass D are similar with only small decreases in the BET specific surface area being observed as the strength of the acid-wash medium was increased (i.e., –3.6 and –9.9%, respectively) as compared with the milled glass. Figure 5 shows that the milled glass D has a broad pore distribution in the 10–80 nm range. On acid washing this distribution of mesopores sharpens to a pore diameter range of

Table 8 Comparison of the influence of acid washing on the BET surface area and the change in the pore volume and diameter of the glasses ($R^2 \geq$ **0.99996)**

Glass	C	Multi-point BET surface area (m^2/g)	Total pore volume (cm^3/g)	Adsorption average pore diameter (nm)	Change in the BET SSA (%)	% Change in pore volume (<23 nm)
A_M	70.65	1.76	0.003	7.66	–	–
A_{AW1}	54.16	2.18	0.004	8.16	23.86	47.18
B_M	87.94	2.02	0.004	7.38	–	–
B_{AW1}	78.31	2.93	0.006	8.82	45.05	129.4
C_M	63.13	2.14	0.004	7.93	–	–
C_{AW1}	89.81	4.36	0.011	9.87	103.74	177.9
D_M	79.22	2.22	0.005	8.13	–	–
D_{AW1}	70.06	2.14	0.004	8.19	–3.6	15.78
D_{AW2}	58.95	2.00	0.004	8.84	–9.9	11.1

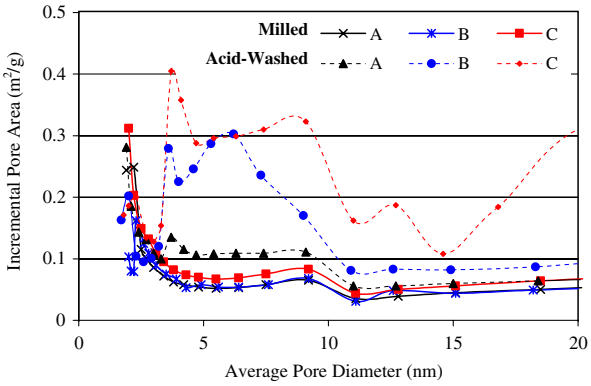

Fig. 4 Comparison of the average pore diameter and incremental pore area distribution of glasses A, B and C (with and without acid treatment)

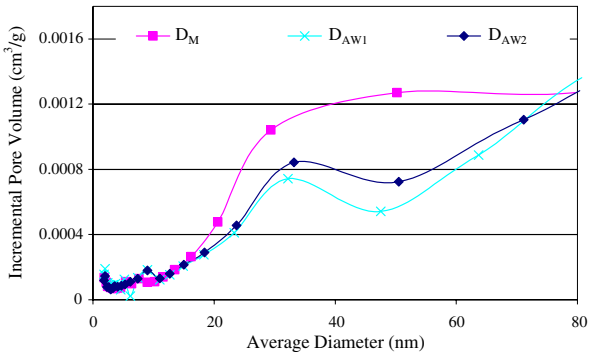

Fig. 5 Comparison of the change in the incremental pore volume with the average pore diameter of glass D following pre- and post-acid washing (Dm = milled glass, D_{AW1} and D_{AW2} = glasses acid washed in 2.5 vol% or 5 vol% glacial acetic acid, respectively)

20–50 nm. This increase in the mesopore volume distribution, however, does not result in an increase in the specific surface area and is therefore possibly associated with a reduction in the surface roughness of the glass.

Susceptibility to changes in the surface morphology of the glasses following acid washing thus appears to be glass composition dependent i.e. the inclusion of sodium in the glass increases the susceptibility of the glass network to surface erosion (glass D) while in the absence of sodium (glasses A, B and C) acid-degradation results in the formation of a mesoporous layer on the surface of the particles that is more pronounced in the low phosphorus containing glass (glass C).

The influence of acid washing on the morphology and composition of the glass surface was also assessed by examining differences in cement working and setting times (Table 9). Acid washing resulted in an increase in the WT and ST of all of the cements with

Table 9 Comparison of the changes in the working and setting time of the cements as a consequence of acid washing

Glass	Working time (s), mean (SD)	Setting time (s), mean (SD)
A_M	84(3)	120(5)
A_{AW1}	331(10)	430(10)
B_M	63(2)	90(0)
B_{AW1}	243(12)	320(5)
C_M	27(1)	nd
C_{AW1}	128(4)	140(6)
D_M	34(1)	nd
D_{AW1}	105(3)	190(4)
D_{AW2}	255(6)	280(8)

the ease of manipulation of the cement paste being glass-composition dependent.

The handling properties of the cement pastes prepared from the glasses showed the WT and ST of the cement pastes produced from glasses A and B and glasses C and D to be similar. XRF data, presented in Table 4, shows glasses A and B to have high phosphate contents (>15 wt%). The mechanism by which the WT and ST of these cements is extended is unclear but may be due to:

- The competitive chelation of released metal cations by liberated phosphate.
- The re-adsorption of phosphate at the glass–solution interface, which has been reported to occur with bioactive glasses in vivo and in vitro although this would not account for the observed differential SIMS release profiles observed.
- An alternative hypothesis is the retention of phosphate within the glass interface to produce a phosphorus–silicon rich depletion-zone where the phosphate behaves as an ion-exchanger retaining metal cations released from the glass and thereby imposing a barrier to ion release. Due to the increase in the phosphate in the network the effective number of network-dwelling metal ions will also increase in order to charge balance the phosphate, which would reduce the number of "free" metal ions able to be leached.

However, the Al:Si ratios of glasses C and D are much greater than their P:Si ratios and therefore the effect of aluminium on the glass network would be expected to dominate that of the phosphate. For glasses C and D the elevated R^{2+}:Al ratios, 3.1 and 3.4, respectively, would result in an increase in the number of network modifier cations that would be readily released. Indeed the cement pastes from milled glasses C and D were unworkable. The slight extension of the WT of the milled glass D may be attributed to

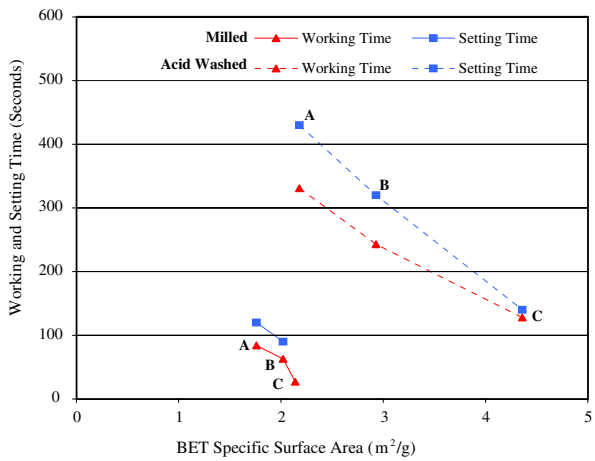

Glass Treatment	Working Time		Setting Time	
	Equation of the Line	R^2	Equation of the Line	R^2
Milled	y = -138.87x + 332.04	0.8757	nd	
Acid Washed	y = -91.441x + 522.65	0.9897	y = -132.08x + 713.61	0.9984

Fig. 6 Influence of glass chemistry and acid washing on the working and setting times of cements A, B and C (n = 3)

the sodium and fluorine contents of the glass which would reduce the influence of the Al:Si and P:Si ratios due to the increase in the number of NBOs incorporated within the glass network thereby promoting dissolution of the glass surface during acid washing and cement paste manipulation.

Comparison of the WT and ST with the glass basicity, CLD, d_{10} and BET SSA infers that it is the BET SSA of the glasses that has the most significant influence on the handling properties of the cement pastes from the glasses A, B and C, which is profoundly influenced by the d_{10}, as illustrated in Figs. 6 and 7.

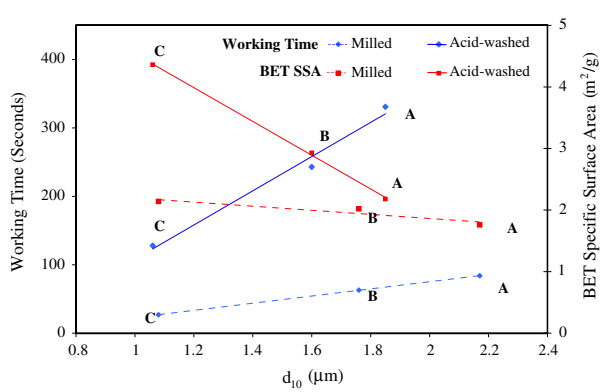

Glass Treatment	Working Time		BET SSA	
	Equation of the Line	R^2	Equation of the Line	R^2
Milled	y = 52.359x – 29.439	0.9999	y = -0.3312x + 2.53	0.8814
Acid Washed	y = 249.92x -141.71	0.9826	y = -2.74x + 7.28	0.9991

Fig. 7 Influence of the d_{10} particle size, glass chemistry and acid washing on the BET SSA of glasses A, B and C and on the working time of cements A, B and C (n = 3)

The supposition of non-stoichiometric leaching from these glasses is supported by SIMS data. For the cements from glass D the converse seems to be true with an increase in the WT as the BET SSA decreases. In conjunction with the rapid rate of set this infers a rapid dissolution of the glass network at the surface of the particles during acid washing and cement mixing with the delay in the WT of the acid washed glasses being due to the diffusional constraints imposed by the formation of a depletion-zone.

4 Conclusions

The influence of glass composition and acid washing on the particle size distributions and surface morphologies of glasses used for preparing GIC pastes has been investigated and effects on working and setting times of cements have been compared. All acid washed glasses had a WT of > 90 s, a BET SSA of between 2.5–6 m^2/g, a d_{50} between 4.4–6.2 mm and a d_{90} of < 20 mm.

- A slight increase in the post-melt Al:Si ratios of the glasses occurs, probably due to the volatilisation of SiF_4 during firing, resulting in a concomitant increase in the acidity of the glass network.
- Acid washing resulted in a decrease in the particle size distribution range of glasses B, C and D, whilst a slight increase in the PSD range was observed following acid washing of glass A, which may be a consequence of particle aggregation or sub-micron particle dissolution.
- The differences between the BET specific surface area of the milled glasses are much smaller than for the acid washed glasses.
- Comparison of the specific surface areas, mathematically modelled by the Mie theory and measured by BET, indicated significant differences in the surface morphology of the acid washed glasses A, B and C. This has been shown to be attributable to changes in the mesopore volume.
- Changes in the mesopore volume also indicated that different mechanisms of acid degradation occur with glass D, which contains sodium, compared with the non-sodium containing glasses A, B and C.
- Acid washing of the glasses used in the preparation of cements increased the working time of the cements by 3- to 7-fold and extended the setting time.
- The working and setting times of the cements prepared from the milled and acid-washed glasses A, B and C decrease with an increase in the BET specific surface areas of the glasses.

- A poor linear correlation between the BET specific surface area of the milled glasses and the working time of their cement pastes was observed despite an excellent correlation between the d_{10} of the milled glass and the working time of the milled glass cement pastes. This indicates that metal cations are rapidly being released from the surface of the milled glasses.
- The reduced working and setting times of the milled glass cement pastes has previously been attributed to the non-stoichiometric leaching of the glass network. From changes in the mesopore volume following acid washing it is proposed that cation rich droplets may be formed throughout the glass network that are highly susceptible to acid leaching and it is the removal of these droplets that gives rise to the mesopore morphology.
- It is also proposed that the phosphate content of the glass has a significant influence on the mesopore volume of acid-washed glasses, for example, glass C, which has reduced phosphate content, shows a marked reduction in the milled glass cement paste working time and nearly a 200% increase in the BET SSA following acid washing.

Acknowledgements The authors gratefully acknowledge Dr. Robert Hill (Dept. of Materials, Imperial College, London) and the assistance of Barry Woodfine (Advanced Healthcare Limited (AHL) (Tonbridge, UK)). Funding for this research was provided under the 5th Framework Programme of the European Union (G5RD CT2001 00475).

References

1. A. D. WILSON and J. W. McLEAN, *Glass-ionomer Cement* (Quintessence Publishing Co., 1988).
2. C. L. DAVIDSON and I. A. MJOR, *Advances in Glass-Ionomer Cements* (Quintessence Publishing Co. Inc., 1999)
3. M. R. TOWLER, A. J. BUSHBY and R. W. BILLINGTON, "Nano-indentation of the glass ionomer/enamel interface in a tooth." *15th European Conference on Biomaterials*, Archon, France (1999) 3#82
4. D. C. SMITH, *Biomaterials* **19**(6) (1998) 467
5. R. J. De MOOR, R. M. VERBEECK and E. A. De MAEYER, *Dental Mater.* **12**(2) (1996) 88
6. G. J. PEARSON, *Clin. Mater.* **7**(4) (1991) 325
7. M. DARLING and R. HILL, *Biomaterials* **15**(4) (1994) 299
8. A. D. WILSON, *Dental Mater.* **12**(1) (1996) 25
9. A. STAMBOULIS, R. V. LAW and R. G. HILL, *Biomaterials* **25**(17) (2004) 3907
10. J. E. SHELBY, *Introduction to Glass Science and Technology* (Cambridge: The Royal Society of Chemistry, 1997)
11. S. G. GRIFFIN and R. G. HILL, *Biomaterials* **21**(7) (2000) 693
12. Y. W. GU and Y. Q. FU, *Thermochim. Acta* **423**(1–2) (2004) 107
13. A. D. NEVE, V. PIDDOCK and E. C. COMBE, *Clin. Mat.* **12**(2) (1993) 113
14. E. A. De MAEYER, R. M. VERBEECK and C. W. VERCRUYSSE, *J. Dent. Res.* **77**(12) (1998) 2005
15. W. SCHMITT, R. PURRMAN, P. JOCHUM and O. GASSER, *United States Patent 4,376,835* (1983).
16. S. B. TURKER and T. BISKIN, *J. Prosthet. Dent.* **89** (2003) 466
17. R. G. Hill, *from internet report: G5RD CT2001 00475* (2004)
18. E. A. De MAEYER, R. M. VERBEECK and C. W. VERCRUYSSE, *J. Dent. Res.* **78** (1999) 1312
19. E. A. WASSON and J. W. NICHOLSON, *Br. Polymer J.* **23** (1990) 179
20. E. A. De MAEYER and R. M. VERBEECK, *J. Dent. Res.* **80** (2001) 1764
21. S. G. GRIFFIN and R. G. HILL, *Biomaterials* **21** (2000) 399
22. C. F. DRAKE and N. R. ADAMS, *German Patent 2,944,687* (1980)
23. S. AKAHANE, S. TOSAKI, K. HIROTA and K. TOMIOKA, *United States Patent 4,900,697* (1990)
24. S. CRISP and A. D. WILSON, *United States Patent 4,143,018* (1979)
25. M. FUKAZAWA, S. MATSUYA and M. YAMANE, *J. Dent. Res.* **69** (1990) 1175
26. L. H. PRENTICE, M. J. TYAS and M. F. BURROW, *Dent. Mater.* **21**(6) (2005) 505.
27. A. MITSUHASHI, K. HANAOKA and T. TERANAKA, *Dent. Mater.* **19**(8) (2003) 747
28. A. E. KAPLAN, J. WILLIAMS, R. W. BILLINGTON, M. BRADEN and G. J. PEARSON, *J. Oral Rehabil.* **31**(4) (2004) 373
29. G. J. FLEMING, A. A. FAROOQ and J. E. BARRALET, *Biomaterials* **24**(23) (2003) 4173
30. S. CRISP and A. D. WILSON, *J. Dent. Res.* **55**(6) (1976) 1023
31. R. G. HILL and A. D. WILSON, *J. Dent. Res.* **67**(12) (1988) 1446.
32. A. TODO, M. HIRASAWA and S. KATO, *United States Patent 6,136,737* (2000).
33. A. T. KUHN and A.D. WILSON, *Biomaterials* **6** (1985) 378
34. J. W. NICHOLSON, *Biomaterials* **19** (1998) 485
35. A. D. WILSON, *J. Mat. Sci. Lett.* **15**(3) (1996) 275
36. S. MATSUYA, T. MAEDA and M. OHTA, *J. Dent. Res.* **75** (1996) 1920
37. T. MAEDA, K. MUKAEDA, T. SHIMOHIRA and S. KATSUYAMA, *J. Dent. Res.* **78**(1) (1999) 86
38. P. V. HATTON and I. M. BROOK, *Br. Dent. J.* **173**(8) (1992) 275
39. ISO13320-1, *Particle Size Analysis: Laser Diffraction Methods* (ISO Standards Authority, 1999)
40. S. J. GREGG and K. S. W. SING, *Adsorption, Surface Area and Porosity* (London: Academic Press, 1982) p. 303.
41. S. BRUNAUER, P. H. EMMETT and E. TELLER, *J. Am. Chem. Soc.* **60** (1938) 309.
42. J. ROUQUEROL, F. ROUQUEROL and K. SING, *Absorption by Powders and Porous Solids* (London: Academic Press Inc., 1998)
43. ISO9917E, *Dental Water-based Cements* (Geneva: International Organisation for Standardisation, 1991)
44. J. H. GIBBS and E. A. DI MARZIO, *J. Chem. Phys.* **28** (1958) 373
45. L. Hench, *Ann. NY Acad. Sci.* **523** (1988) 54
46. A. RAVAGLIOLO and A. KRAJEWSKI, *Bioceramics* (Chapman and Hall, 1992)